Synthesis, Crystal Structure, and Magnetic Properties of $Mn_2(OH)_2SO_4$: A Novel Layered Hydroxide

Mohsen Ben Salah,[a] Serge Vilminot,*[a] Tahar Mhiri,[b] and Mohamedally Kurmoo[a]

Keywords: Hydroxysulfate / Hydrothermal synthesis / Magnetic properties / Manganese

$Mn_2(OH)_2SO_4$, obtained as pink prismatic crystals by the hydrothermal reaction of $MnSO_4 \cdot H_2O$ and NaOH at 240 °C for 24 h, consists of layers of Mn hydroxide connected to each other through μ^6-sulfate ions. Each layer exhibits vacancies, and each vacant space is capped at the top and bottom by the sulfate groups. The compound is paramagnetic above 50 K (C = 4.36 emu K mol^{-1}, μ_{eff} = 5.91 μ_B, Θ = −100 K). Below 45 K, the magnetization increases slightly, indicating canted-antiferromagnetic ($T_{Néel}$ = 42±1 K) behavior consistent with the linear dependence of the magnetization as a function of the field at 2 K, which reaches only 0.4 μ_B at 50 kOe, and the lack of any imaginary component of the ac-susceptibilities (ac = alternating current).

Introduction

Layered compounds have attracted continuing interest in many different fields of research.[1] The principal interest, in the early days, was due to their applications resulting from their sorption properties and, therefore, for selective separation, ion exchange chromatography, and as electrodes. These applications developed to include catalysis, since they have quite large surface areas, and also photopolymerization.[2] More recently, these materials have been of interest as a result of their magnetism, especially as models for low dimensional behavior in antiferromagnets but also for understanding the exchange mechanism through space when the layers are separated by non-magnetic intercalants.[3,4]

From a synthetic chemistry point of view, the layered compounds are very difficult to obtain as single crystals, and in cases where crystals of a few tens of nanometers in size have been obtained, resolution of the crystal structures was hampered by several dislocations and stacking faults, for example turbostratic faults.[5] Using hydrothermal techniques it has been possible to obtain a few compounds as single crystals.[6,7] Consequently, for those with crystal sizes large enough, their crystal structures were determined. In a few cases, the structures have been determined by Rietveld refinement of high-quality powder diffraction data.[8,9] Furthermore, certain disorders were fully characterized in some cases.[7,10]

Amongst the hydroxides of the divalent cations, the layer topology can be quite variable. The simplest case is that of brucite, which is adopted by the transition metal hydroxides $M(OH)_2$.[11−12] Variants of these are formed by replacing some of the hydroxides by other anions, such as $Cu_2(OH)_3NO_3$.[13] In the literature, these have been classified as β- and α-phases, respectively. A further modification of the layer topology can be achieved by periodically replacing some of the octahedra within the brucite layer, and capping the vacant sites by tetrahedrally coordinated MO_4 units. Examples of these are $Zn_5(OH)_8(H_2O)_2(NO_3)_2$,[14] $Zn_5(OH)_8Cl_2 \cdot H_2O$,[15] $Co_5(OH)_8(C_8H_{10}O_4) \cdot 4H_2O$,[7] and $Co_8(OH)_{12}(SO_4)_2(\text{pillar}) \cdot xH_2O$ {pillar = 1,2-diaminoethane or 4,4′-diazabicyclo[2.2.2]octane (dabco); x = 3 or 1}.[10] These structures are only observed for Zn and Co since both metals adopt a four-coordinate geometry. A more exotic layer topology can be found for $Co_2(OH)_2$(terephthalate),[9] which adopts a topology similar to the 110 planes of normal rutile, i.e. consisting of edge-sharing chains of octahedra connected to similar chains through the apices of the octahedra with the layers being interleaved by the bridging dianionic terephthalate. A further variant was found for $M_2(OH)_2(C_2O_4)$ (M = Co or Mn), which consists of dimers of edge-sharing octahedra connected to one another by their apices thus forming corrugated layers. These layers are then connected by the oxalate ions.[16] $Mn(OH)(OAc)_2 \cdot HOAc$ is an interesting layered compound employing both coordination and hydrogen bonds.[17]

In this paper we present the synthesis, crystal structure, and characterization by IR spectroscopy and DT-TGA of $Mn_2(OH)_2SO_4$. It displays a novel layered topology and be-

[a] Groupe des Matériaux Inorganiques, IPCMS, UMR 7504 (ULP-CNRS),
23 rue du Loess, B. P. 43, 67034 Strasbourg Cedex 2, France
E-mail: vilminot@ipcms.u-strasbg.fr
[b] Laboratoire de l'État Solide, Faculté des Sciences,
3038 Sfax, Tunisia

Supporting information for this article is available on the WWW under http://www.eurjic.org or from the author.

  DOI: 10.1002/ejic.200300909

haves as a paramagnet above 50 K with a long-range Néel transition at 42 K, and the appearance of a weak magnetization due to a very small canting.

Results and Discussion

X-ray Diffraction

X-ray powder diffraction data collected on the pink crystals confirmed the formation of a new phase. The diffraction lines were indexed from the unit cell parameters measured on a single crystal using the pattern-matching mode of FULLPROF.[20] All lines were then indexed confirming, that the sample was a single phase. Figure S1 (see Supporting Information) gives the corresponding diffractogram.

Thermal Analysis

The TGA trace (Figure S2, Supporting Information) revealed that the decomposition takes place in three steps. The first step between 300 and 500 °C associated with an endothermic effect on the DTA trace, whose maximum is at 497 °C, can be attributed to the loss of hydroxy groups as water. The second step between 780 and 870 °C (endothermic effect at 862 °C) is related to the decomposition of the sulfate groups to SO_3. In the final step, weight loss at around 910 °C (endothermic at 912 °C) corresponds to the reduction of the manganese oxide previously formed at lower temperatures. Starting from an Mn^{II} compound, it is well known that the corresponding MnO oxide is not stable and will be transformed into Mn_2O_3. The corresponding oxidation reaction is well identified by the weight increase between 600 and 700 °C, and by the weight loss value between 780 and 870 °C, which is lower than predicted if MnO were to be stable. The experimental Mn content, 44.9 wt%, is in good agreement with the expected value of 45.8 wt%.

Structure Description

The structure is built up of a succession of layers parallel to the *bc* plane, alternating between layers containing MnO_6 octahedra, and layers containing SO_4 tetrahedra (Figure 1). Each tetrahedron shares its four corners with six different octahedra, three on each adjacent layer. Inside an $(MnO_6)_n$ layer, each octahedron shares its edges with three neighboring octahedra, and is further corner-shared with one octahedron. This results in a layer with apparent porosity (Figure 2). In the brucite layers, each octahedron is surrounded by six octahedra resulting in a full occupation of the layer space. The MnO_6 octahedra are distorted with three Mn−OH distances between 2.113 and 2.169 Å, and three Mn−O(sulfate) distances between 2.258 and 2.318 Å. Moreover, the interatomic angles also differ from the values expected for a regular octahedron, with values as low as 152° instead of 180°, and 117° instead of 90°. On the other hand, the sulfate tetrahedra are almost regular. OH and O(2) oxygen atoms are of the μ^3-type, OH being bonded to three Mn ions, and O(2) to two Mn centers and one S atom, whereas O(1) is a μ^2-oxo group, and is bonded to one Mn and one S atom. The O−H bond length of 0.77 Å is in agreement with the distances usually found from X-ray diffraction data. The H atom participates in a very weak hydrogen bond with O(1) with an H···O(1) distance of 2.12 Å. Bond valence calculations using the model of Brown and Altermatt[21] reveal, that values (Table 1) close to those expected are obtained for S, Mn and O2. For O1 and OH, the observed deviations are probably related to the uncertainty of the O−H and H···O(1) bond lengths.

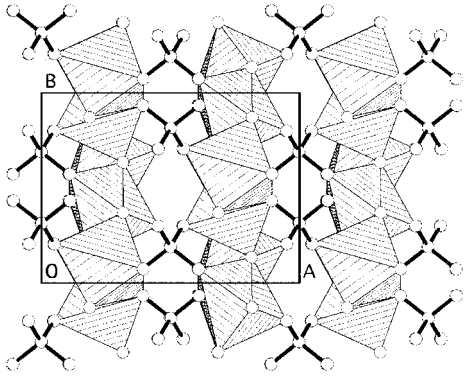

Figure 1. Projection of the structure along the *c* axis (perpendicular to the stacking axis) showing the connections between the layers by the sulfate ions; manganese atoms are presented as polyhedra and the sulfates as spheres and sticks

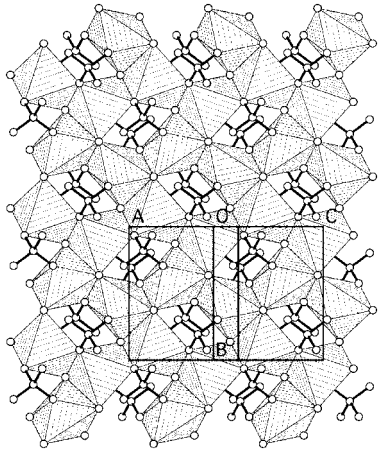

Figure 2. Projection of the structure perpendicular to the layers showing the vacancies, which are coordinated at the top and bottom by the sulfate ions

The required number of Mn−O bonds per formula unit is 12. This requirement is satisfied by the presence of three bonds from each hydroxide ion, and six bonds from the sulfate group. This is similar to that observed for $M_2(OH)_2C_2O_4$ (M = Mn or Co), and for $Co_2(OH)_2$(terephthalate) where, in both cases, the hydroxide ions are both μ^3-bridging and the carboxylate ion forms six bonds with

Table 1. Bond valence calculations

	O(1)	O(2)	OH	OH	OH	H	S	Mn	Σs[a]
S	1.512	1.440							5.904
	1.512	1.440							
Mn	0.282	0.262	0.418	0.397	0.359				1.958
		0.240							
O(1)						0.035	1.512	0.282	1.829
O(2)							1.440	0.262	1.942
								0.240	
OH						1.354		0.418	2.528
								0.397	
								0.359	
H	0.035		1.354						1.389

[a] $s = \exp[(r_0 - r)/B]$ with $r_0(S) = 1.624$, $r_0(\mathrm{Mn}) = 1.790$, $r_0(\mathrm{H}) = 0.882$, $B = 0.37$ from ref.[21]

the surrounding metal atoms.[9,16] Such a μ^6-coordination for the sulfate is rare (Figure 3), it is commonly found as an independent anion, or displaying single-, μ^2-, μ^3- or μ^4-coordination.

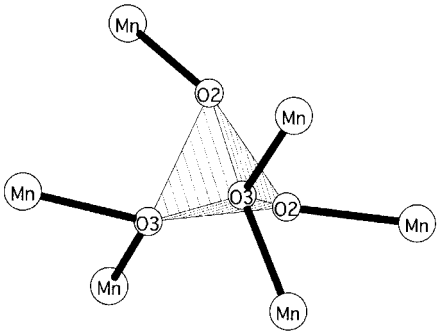

Figure 3. The six-fold coordination of the sulfate group

Infrared Spectroscopy

The infrared spectrum recorded between 500 and 4000 cm^{-1} (Figure S3, Supporting Information) exhibits vibrational bands related to the O−H and S−O bonds. The first ones are near 3500 cm^{-1} as well as in the 900−650 cm^{-1} region, whereas the second ones are near 1100 and 600 cm^{-1}.[22] The sharp band with its maximum at 3498 cm^{-1} can be attributed to the O−H stretching mode of the OH group. Its sharpness is related to the presence of an OH group not involved in hydrogen bonding as revealed by the structural data. The ν_3 and ν_4 vibrational bands of the sulfate group appear as doublets at 1153−1105 cm^{-1} and 617−603 cm^{-1}, respectively. The presence of two bands is related to the local symmetry of the tetrahedron.

Magnetic Susceptibility

In the paramagnetic region, the magnetic susceptibility measured on a randomly oriented sample, consisting of few selected washed crystals, follows the Curie−Weiss law, $\chi = C/(T - \theta) = 8.72/(T + 100)$ emu mol^{-1}, where the Curie and Weiss constants were obtained by fitting the $1/\chi$ experimental data in the temperature range 150−300 K (Figure 4). The negative θ value indicates that the dominant nearest neighbor exchange interactions within the layer are antiferromagnetic. From the Curie constant, $C = Ng^2\mu_B{}^2s(s + 1)/3k$, of 4.36 emu K per Mn and $s = 5/2$, we deduced a value of the Landé g factor of 1.997, in good agreement with a ^{6}A ground state ion. The effective moment $(8C)^{1/2}$ of 5.907 μ_B is close to the expected value of 5.92 μ_B, calculated with the spin-only formula.[23] It appears that the severe distortion of the MnO_6 octahedron has little effect on the moment. On lowering the temperature, χ exhibits a sharp increase starting around 45 K before reaching a plateau down to the lowest temperature. On the χT curve, a maximum can be detected at the previously mentioned temperature of 42 K before decreasing to a value close to zero at 4 K. This behavior has been attributed to the presence of a 3D-antiferromagnetic ordering below the Néel temperature $T_N = 42$ K. The sharp increase at 45 K may be due to a small canting of the sub-lattice. To verify that this anomaly is not due to a small amount of impurity, we performed the experiment on a clean single crystal and observed the same transition (Figure S4, Supporting Information). If we assume that the magnetic unit cell is the same as the nuclear one, that is with a propagation vector k (0,0,0),[24] we may therefore expect an antiferromagnetic ordering due to the presence of the center of symmetry. The isothermal magnetization at 2 K (Figure 5) shows a linear dependence and reaches 0.4 μ_B in a field of 50 kOe. Such behavior is consistent with long-range antiferromagnetic ordering. However, the near-zero residual magnetization indicates the canting angle is immeasurably small. A broad maximum in the real component of the ac-susceptibility (Figure 6) is consistent with the antiferromagnetic coupling, and long-range antiferromagnetism. Due to the very small canting angle, there is no imaginary component in the ac-susceptibility as a function of temperature. Using the moment (M_{2K}) at 2 K in an applied field of 100 Oe, we estimated the canting angle, $\sin^{-1}(M_{2K}/M_s) = \sin^{-1}(6.7/2 \times 5 \times 5585)$, to be $7{\cdot}10^{-3}$ °.

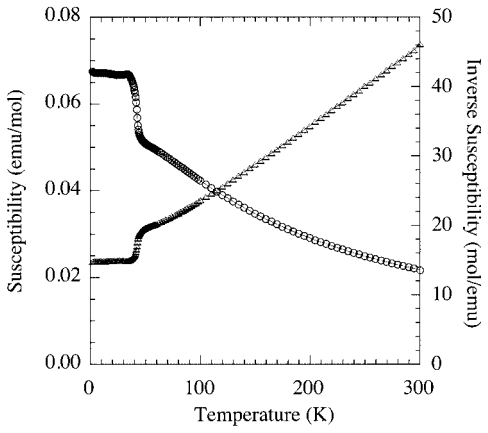

Figure 4. Temperature dependence of the dc-susceptibility (circles), and the inverse dc-susceptibility (triangles) of a polycrystalline sample measured in an applied field of 100 Oe

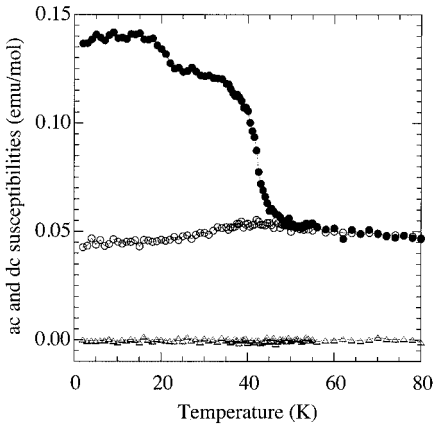

Figure 5. dc-Susceptibility (filled circles) on cooling in an applied dc-magnetic field of 2 Oe, and ac-susceptibilities (circles for the real, and triangles for the imaginary component) in an applied ac-field of 1 Oe oscillating at 17 Hz

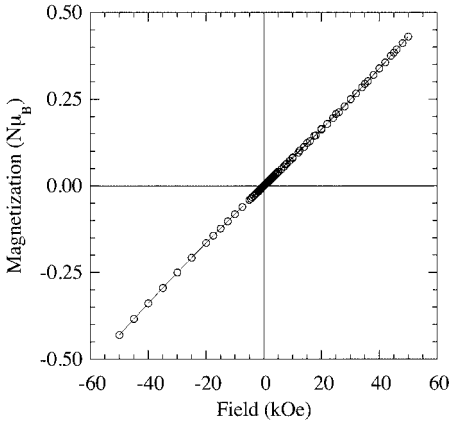

Figure 6. Isothermal magnetization at 2 K of a polycrystalline sample

Conclusion

High-quality crystals of $Mn_2(OH)_2SO_4$ were prepared as a minority phase by the hydrothermal reaction of $MnSO_4{\cdot}H_2O$ and NaOH. It displays a novel layered topology, and a canted-antiferromagnetic state below the Néel temperature of 42 K.

Experimental Section

Synthesis: $Mn_2(OH)_2SO_4$ was obtained by a hydrothermal synthesis. $MnSO_4{\cdot}H_2O$ (2.5 g, 14.8 mmol) and sodium hydroxide (0.7 g, 17.5 mmol) were separately dissolved in boiling distilled water (20 mL), and the two solutions were quickly mixed while still hot. The resultant suspension was immediately poured into the autoclave, which was then sealed and heated at 240 °C for 24 h under autogenous pressure. Under these conditions, a mixture of $Mn_3(OH)_2(SO_4)_2(H_2O)_2$[18] and $Mn_2(OH)_2SO_4$ was obtained. Several attempts to promote the formation of a single phase by varying the starting Mn/Na proportions, and the conditions of the hydrothermal synthesis (temperature, time, dilution) were unsuccessful. Fortunately, the crystal habits and colors of the two phases are quite different. It was therefore possible to separate the phases using an optical microscope. Whereas $Mn_3(OH)_2(SO_4)_2(H_2O)_2$ crystallizes as pale beige platelets, $Mn_2(OH)_2SO_4$ appears as larger pink prismatic crystals, which were easily separated. Following separation, the crystals were washed with acetone in an ultrasonic bath to remove small traces of the other phase and finally dried in air.

Characterization: The thermal analysis was performed with a TA-STD-Q600 apparatus, at a 3 °C/min heating rate, under air. Infrared spectra were recorded with an ATI Mattson spectrometer by transmission through KBr pellets containing 1% of the crystals. Powder X-ray diffraction patterns were recorded using a D5000 Siemens diffractometer equipped with a back monochromator (Cu-$K_{\alpha 1}$, 1.5406 Å). For X-ray data collection, a single crystal was selected and mounted on a glass fiber. A single set of 180 frames, 20 s/frame, scan of 1°/frame (each frame measured twice), crystal−detector distance = 30 mm, θ = 0°, κ = 0°, was collected at room temperature with a Nonius Kappa CCD diffractometer at the Service Commun de Rayons X, Université Louis Pasteur, Strasbourg. The structure was solved by means of a three-dimensional Patterson function allowing location of the positions of the manganese atoms. Subsequent parameter refinement cycles and three-dimensional difference Fourier maps using SHELXS-93[19] yielded the positions of all the other atoms. The final refinement included anisotropic displacement parameters, and a secondary extinction correction. The atomic coordinates of hydrogen atoms were isotropically refined. Additional experimental details are given in Table 2 and in the Supporting Information. Table 3 gives the final atomic positions and Table 4 the corresponding bond lengths and angles. The oxygen atoms of the sulfate and hydroxy groups have been labeled as O and OH, respectively. Further details of the crystal-structure investigation may be obtained from the Fachinformationszentrum Karlsruhe, 76344 Eggenstein-Leopoldshafen, Ger-

Table 2. Summary of the single-crystal X-ray data collection and structural refinement of $Mn_2(OH)_2SO_4$

a [Å]	11.2358(5)	μ [mm^{-1}]	5.58
b [Å]	7.4822(4)	hkl range	$-15 < h < 16$
c [Å]	6.1572(3)		$-9 < k < 10$
			$-8 < l < 8$
		θ range [°]	1−31
β [°]	115.061(3)	Total number of reflections	1229
V [Å^3]	468.90(8)	Unique reflections	738
Z	4	Unique $\lvert I_o\rvert > 2\sigma(I_o)$	655
Space group	$C2/c$ (no. 15)	R_{int} [%]	2.9
F (000)	448.0	R_F (all data) [%]	3.46
$D_{calcd.}$ [g·cm^{-3}]	3.399	$wR2(F_o^2)$ (all data) [%]	7.4
Radiation λ [Å]	0.71703	GoF [%]	1.105

Table 3. Fractional atomic coordinates for $Mn_2(OH)_2SO_4$ obtained from X-ray data at 295 K

Atom	x/a	y/b	z/c
Mn	0.25127(3)	0.09849(5)	0.18252(6)
S	0	0.31357(12)	0.25
OH	0.3147(2)	0.3689(3)	0.2011(3)
O1	0.0490(2)	0.2023(3)	0.1084(3)
O2	0.1087(2)	0.4293(3)	0.4143(3)
H	0.390(5)	0.359(5)	0.275(8)

Table 4. Interatomic distances [Å] and angles [°] from the X-ray structure determination

S−O1	1.471(2) × 2	O1−S−O1	111.0(3)	O2−S−O2	108.9(2)
S−O2	1.489(2) × 2	O1−S−O2	109.1(3) × 2	<O−S−O>	109.5
<S−O>	1.480	O1−S−O2	109.4(3) × 2		
Mn−OH	2.113(2)	OH−Mn−OH	155.61(4)	OH−Mn−O2	88.16(7)
Mn−OH	2.132(2)	OH−Mn−OH	116.99(7)	OH−Mn−O1	83.73(7)
Mn−OH	2.169(2)	OH−Mn−O1	83.13(7)	OH−Mn−O2	74.58(7)
Mn−O1	2.258(2)	OH−Mn−O2	90.99(7)	OH−Mn−O2	160.11(4)
Mn−O2	2.286(2)	OH−Mn−O2	74.94(8)	O1−Mn−O2	151.96(7)
Mn−O2	2.318(2)	OH−Mn−OH	84.47(7)	O1−Mn−O2	114.56(7)
<Mn−O>	2.213	OH−Mn−O1	88.26(7)	O2−Mn−O2	89.99(7)
		OH−Mn−O2	106.73(7)		
OH−H	0.77(5)	H···O1	2.12(5)	OH−H···O1	148

many, on quoting the depository number CSD-413556 (they can be requested from Crysdata@FIZ-Karlsruhe.de).

[1] [1a] R. Schollhorn, *Intercalation Compounds*, Academic Press, London, **1984**. [1b]A. Clearfield, *Chem. Rev.* **1988**, *88*, 125. [1c] A. J. Jacobsen, *Intercalation Reactions of Layered Compounds* in *Solid State Chemistry: Compounds* (Eds.: P. Day and A. Cheetham), Oxford University Press, Oxford, **1992**. [1d] D. O'Hare, *Inorganic Intercalation Chemistry* in *Inorganic Materials* (Eds.: D. W. Bruce and D. O'Hare), Wiley, London, **1993**. [1e]A. Clearfield, *Curr. Opin. Solid State Chem.* **1996**, *1*, 268. [1f] A. Clearfield, *Inorganic Ion Exchange Materials* (Ed.: A. Clearfield), CRC Press Inc., Boca Raton, Florida, **1991**.

[2] [2a] T. Pinnavaia, *Science* **1983**, *220*, 365. [2b] T. Shichi, K. Takagi, Y. Sawaki, *Chem. Commun.* **1996**, 2027.

[3] *Magnetic Properties of Layered Transition Metal Compounds* (Ed.: L. J. De Jongh), Kluwer Academic Publishers, Dordrecht, **1990**.

[4] M. Kurmoo, *Phil. Trans. R. Soc., Lond.* **1999**, *357*, 3041; M. Kurmoo, *Chem. Mater.* **1999**, *11*, 3370; M. Kurmoo, *J. Mater. Chem.* **1999**, *9*, 2595; M. Kurmoo, P. Day, A. Derory, C. Estournes, R. Poinsot, M. J. Stead, C. J. Kepert, *J. Solid State Chem.* **1999**, *145*, 452.

[5] [5a] I. V. Mitchell, *Pillared Layered Structures; Current Trends and Applications*, Elsevier, London, **1990**. [5b]S. Carlino, *Solid State Ionics* **1997**, *98*, 73.

[6] A. Rabenau, *Angew. Chem. Int. Ed. Engl.* **1985**, *24*, 1026.

[7] M. Kurmoo, H. Kumagai, S. M. Hughes, C. J. Kepert, *Inorg. Chem.* **2003**, *42*, 6709.

[8] H. M. Rietveld, *J. Appl. Crystallogr.* **1969**, *2*, 65−71.

[9] M. Kurmoo, H. Kumagai, M. A. Green, B. W. Lovett, S. J. Blundell, A. Ardavan, J. Singleton, *J. Solid State Chem.* **2001**, *159*, 343.

[10] A. Rujiwatra, C. J. Kepert, J. B. Claridge, M. J. Rosseinsky, H. Kumagai, M. Kurmoo, *J. Am. Chem. Soc.* **2001**, *123*, 10584.

[11] H. R. Oswald, R. Asper in *Preparation and Crystal Growth of Materials with Layer Structures* (Ed.: R. M. A. Leith), Reidel, Dordrecht, **1977**, p. 71.

[12] C. Mockenhaupt, T. Zeiske, H. D. Lutz, *J. Mol. Struct.* **1998**, *443*, 191.

[13] [13a] H. L. Wells, S. L. Penfeld, *Am. J. Sci.* **1885**, *30*, 50. [13b] B. Bovio, S. Locchi, *J. Crystallogr. Spectr. Res.* **1982**, *12*, 507. [13c] H. Effenberger, *Z. Kristallogr.* **1983**, *165*, 127.

[14] W. Stahlin, H. R. Oswald, *Acta Crystallogr., Sect. B* **1970**, *26*, 860.

[15] R. Allmann, *Z. Kristallogr.* **1968**, *126*, 417.

[16] [16a] D. Price, F. Lionti, R. Ballou, P. T. Wood, A. K. Powell, *Phil. Trans. R. Soc., Lond.* **1999**, *A357*, 3099. [16b] Z. A. D. Lethbridge, A. F. Congreve, E. Esslemont, A. M. Z. Slawin, P. Lightfoot, *J. Solid State Chem.* **2003**, *172*, 212.

[17] D. J. Price, S. R. Batten, B. Moubaraki, K. S. Murray, *Polyhedron* **2003**, *22*, 2161.

[18] [18a] M. Ben Salah, S. Vilminot, G. André, M. Richard-Plouet, F. Bourée-Vigneron, T. Mhiri, M. Kurmoo, *Chem. Eur. J.*, in press. [18b]S. Vilminot, M. Richard-Plouet, G. André, D. Swierczynski, F. Bourée-Vigneron, M. Kurmoo, *Inorg. Chem.* **2003**, *42*, 6859.

[19] G. M. Sheldrick, *SHELXL*-93, *Program for the Refinement of Crystal Structures*, University of Göttingen, Germany, **1993**.

[20] J. Rodriguez-Carvajal, *FULLPROF: Rietveld, Profile Matching and Integrated Intensity Refinement of X-ray andlor Neutron Data*, ver. 3.5d, Léon-Brillouin Laboratory, CEA Saclay, France, **1998**.

[21] I. D. Brown, D. Altermatt, *Acta Crystallogr., Sect. B* **1985**, *41*, 244−247.

[22] K. Nakamoto, *Infrared and Raman Spectra of Inorganic and Coordination Compounds*, John Wiley, New York, **1986**.

[23] A. Herpin, *Theorie du Magnetisme*, Presse Universitaire de France, Paris, **1968**.

[24] E. F. Bertaut, *Acta Crystallogr., Sect. A* **1968**, *24*, 217.

Received December 8, 2003
Early View Article
Published Online April 7, 2004

